Hyperspectral versus multispectral remote sensing approach to detect phytoplankton blooms in coastal waters : application to a Phaeocystis bloom.

B. Lubac, Hubert Loisel, N. Guiselin, R. Astoreca, Luis Felipe Artigas, X. Mériaux.

Hyperspectral and multispectral ocean color inversions to detect *Phaeocystis globosa* blooms in coastal waters

Bertrand Lubac,[1] Hubert Loisel,[1] Natacha Guiselin,[1] Rosa Astoreca,[2] L. Felipe Artigas,[1] and Xavier Mériaux[1]

Received 16 July 2007; revised 15 February 2008; accepted 28 February 2008; published 26 June 2008.

[1] Identification of phytoplankton groups from space is essential to map and monitor algal blooms in coastal waters, but remains a challenge due to the presence of suspended sediments and dissolved organic matter which interfere with phytoplankton signal. On the basis of field measurements of remote sensing reflectance ($R_{rs}(\lambda)$), bio-optical parameters, and phytoplankton cells enumerations, we assess the feasibility of using multispectral and hyperspectral approaches for detecting spring blooms of *Phaeocystis globosa* (*P. globosa*). The two reflectance ratios ($R_{rs}(490)/R_{rs}(510)$ and $R_{rs}(442.5)/R_{rs}(490)$), used in the multispectral inversion, suggest that detection of *P. globosa* blooms are possible from current ocean color sensors. The effects of chlorophyll concentration, colored dissolved organic matter (*CDOM*), and particulate matter composition on the performance of this multispectral approach are investigated via sensitivity analysis. This analysis indicates that the development of a remote sensing algorithm, based on the values of these two ratios, should include information about *CDOM* concentration. The hyperspectral inversion is based on the analysis of the second derivative of $R_{rs}(\lambda)$ ($d\lambda^2 R_{rs}$). Two criteria, based on the position of the maxima and minima of $d\lambda^2 R_{rs}$, are established to discriminate the *P. globosa* blooms from diatoms blooms. We show that the position of these extremes is related to the specific absorption spectrum of *P. globosa* and is significantly correlated with the relative biomass of *P. globosa*. This result confirms the advantage of a hyperspectral over multispectral inversion for species identification and enumeration from satellite observations of ocean color.

Citation: Lubac, B., H. Loisel, N. Guiselin, R. Astoreca, L. Felipe Artigas, and X. Mériaux (2008), Hyperspectral and multispectral ocean color inversions to detect *Phaeocystis globosa* blooms in coastal waters, *J. Geophys. Res.*, *113*, C06026, doi:10.1029/2007JC004451.

1. Introduction

[2] Since the first maps of chlorophyll concentration were obtained from ocean color data collected by the Coastal Zone Color Scanner (CZCS) onboard the Nimbus 7 satellite (1978–1986) [*Feldman et al.*, 1989], the oceanographic community is in a permanent quest for novel ocean color products to study and constrain physical, biological, and chemical processes in the ocean. The identification of phytoplankton taxonomic groups from space is a major thrust for a variety of reasons. First, knowledge of the global distribution of the main plankton functional types may greatly enhance our understanding on the oceanic carbon cycle and on the marine ecosystem [*Platt et al.*, 2003; *Smith et al.*, 2002; *Le Quéré et al.*, 2005]. Second, mapping and monitoring of harmful algal blooms associated with specific phytoplankton can help prevent human health threat, assist in fisheries management, and assist the tourism industries [*Cullen et al.*, 1997; *Stumpf et al.*, 2003; *Tomlison et al.*, 2004; *Craig et al.*, 2006]. Finally, episodic blooms may also contribute to bias the remote sensing estimation of various components of seawater, such as colored dissolved organic matter (*CDOM*), suspended particulate matter (*SPM*), and chlorophyll *a* concentration (*Chl*) [*Sathyendranath et al.*, 2001; *Bouman et al.*, 2003; *Alvain et al.*, 2006].

[3] During the last decade, several techniques were developed for remote detection and identification of phytoplankton blooms. Some of them use the spectral signature of the phytoplankton inherent optical properties (IOPs), and in particular of the phytoplankton absorption coefficient ($a_\phi(\lambda)$) [*Johnsen et al.*, 1994; *Millie et al.*, 1997; *Staer and Cullen*, 2003; *Sathyendranath et al.*, 2004; *Westberry et al.*, 2005]. For example, *Sathyendranath et al.* [2004] and *Westberry et al.* [2005] developed semi-analytical models to detect diatoms and the cyanobacterium *Trichodesmium* spp., respectively, from multispectral sensors. Other algorithms directly exploit the multispectral or hyperspectral patterns of the remote sensing reflectance ($R_{rs}(\lambda)$) without using an explicit inversion. For example, *Alvain et al.* [2005] devel-

[1]Université du Littoral Côte d'Opale, Laboratoire d'Océanologie et de Géosciences (LOG), Wimereux, France.
[2]Université Libre de Bruxelles, Ecologie des Systèmes Aquatiques (ESA), Brussels, Belgium.

0148-0227/08/2007JC004451

oped multispectral classification schemes to assess four different groups of phytoplankton (haptophytes, *Prochlorococcus*, *Synechococcus*, and diatoms) from space. *Craig et al.* [2006] explored the hyperspectral approach and developed a method to detect *Karenia brevis* from $R_{rs}(\lambda)$. This method is based on the similarity index analysis of the $a_\phi(\lambda)$ spectrum [*Millie et al.*, 1997], this last being derived from $R_{rs}(\lambda)$ using a quasi-analytical algorithm.

[4] Most of the studies dedicated to remote detection and characterization of phytoplankton blooms were principally developed for "case 1" waters; that is for waters where IOPs variations are mainly due to phytoplankton and its covarying material [*Morel and Prieur*, 1977]. Only a few algorithms deal with coastal waters in which the presence of suspended sediments and dissolved organic matter of terrestrial origin interfere with the phytoplankton attributed radiometric signal. *Subramaniam et al.* [2002] demonstrated that their semi-empirical classification scheme may be applied to coastal waters. In a similar way, *Craig et al.* [2006] showed that their method is not significantly affected by varying *CDOM* concentration. Despite all this progress, identification of taxonomic groups in coastal waters remains a challenge, in particular in waters where *SPM*, *CDOM* and phytoplankton all vary independently as in western European waters.

[5] In the eastern English Channel and southern North Sea, a region characterized by typical coastal processes, blooms of the prymnesiophyceae *Phaeocystis globosa* (*P. globosa*) occur nearly every spring, generally following a first bloom of diatoms. *P. globosa* is characterized by a complex polymorphic life cycle alternating free living cells (3–9 μm in diameter) and gelatinous colonies (100 μm up to 3 mm), which can lead to accumulations of mucilaginous aggregates (foam) at the sea surface and on beaches [*Rousseau et al.*, 1994; *Schoemann et al.*, 2005]. *P. globosa* blooms have a considerable impact on the ecosystem and water quality [*Hamm*, 2000; *Veldhuis and Wassman*, 2005]. Recent research has shown that diatoms and prymnesiophytes can be partially discriminated from optical measurements. *Stuart et al.* [2000] distinguished these two groups from their spectral signatures in phytoplankton absorption, $a_\phi(\lambda)$, and they showed that the spectral dissimilarities were directly related to their pigment composition. *Astoreca et al.* [2005] and *Astoreca* [2007] showed that the second and fourth derivatives of the absorption spectra of these two algal populations present specific differences at 467 and 500 nm. Finally, *Lubac et al.* [2005] showed that the $R_{rs}(\lambda)$ spectra and their second derivatives associated with *P. globosa* blooms have a sufficiently unique spectral signature to be detected from hyperspectral $R_{rs}(\lambda)$ measurements.

[6] In this paper, we investigate the potential offered by both hyperspectral and multispectral measurements of $R_{rs}(\lambda)$ to identify *P. globosa* blooms from remote sensing. This study is based on a data set gathered in situ that includes: $R_{rs}(\lambda)$ spectra, bio-optical, and biogeochemical parameters, as well as laboratory-based phytoplankton cell enumerations. All data were acquired from field cruises carried out in the eastern English Channel and southern North Sea. The hyperspectral inversion method is based on the analysis of the second derivative of $R_{rs}(\lambda)$ to establish two criteria to discriminate *P. globosa* from diatoms. Results are compared with those of a similarity index analysis performed on the phytoplankton absorption spectra, $a_\phi(\lambda)$. The multispectral inversion is developed using the spectral bands available on current ocean color sensors. A sensitivity analysis is performed to test the effects of the different optically significant parameters on the two reflectance ratios used in this multispectral approach. This analysis is crucial for providing guidance to when the inversion is likely to work using ocean color.

2. Data and Methods

2.1. Description of the Field Campaigns

[7] Intensive field measurements were performed from March to June 2004 in the inshore and offshore waters of the eastern English Channel and southern North Sea. The stations sampled during the cruise periods (15–18 March, 11–15 April, 10–15 May, 25–30 June) are displayed in Figure 1. The investigated area is affected by typical coastal processes such as a large tidal range, sediment resuspension, mixing of various water masses, freshwater inputs, and a succession of intense spring blooms of diatoms and *P. globosa* [*Breton et al.*, 2000; *Sazhin et al.*, 2007]. All these processes are responsible for the high variability of IOPs [*Vantrepotte et al.*, 2007; *Loisel et al.*, 2007] and $R_{rs}(\lambda)$ [*Lubac and Loisel*, 2007] in time and space. Although the algal community is very mixed in this region, *Vantrepotte et al.* [2007] showed that the phytoplankton biomass is greatly (from 80 to 90 %) dominated by diatoms and *P. globosa* from March to June.

2.2. Remote Sensing Reflectance Measurements

[8] Hyperspectral (3 nm resolution) radiometric measurements were performed in the 350–750 nm spectral range with two TriOS radiometers. A full description of the radiometric data processing is given by *Lubac and Loisel* [2007]. The first radiometer (on the deck) measured the above-surface downward irradiance ($E_d(0^+, \lambda)$) and the second (in-water) measured the profile in the water column of the upward radiance ($L_u(z, \lambda)$). Calibrated data for $E_d(0^+, \lambda)$ and $L_u(z, \lambda)$ were interpolated to 2.5 nm intervals. Remote sensing reflectance ($R_{rs}(\lambda)$) was then calculated from the *in-water* method, following the protocols prescribed by *Mueller* [2003]:

$$R_{rs}(\lambda) = \frac{L_w(\lambda)}{E_d(0^+, \lambda)} \quad (1)$$

where the water-leaving radiance ($L_w(\lambda)$) is obtained after extrapolation of $L_u(z, \lambda)$ just below the surface to determine $L_u(0^-, \lambda)$ and its transmission through the air-sea interface ($L_w(\lambda) = 0.543 \times L_u(0^-, \lambda)$). To limit impact of external factors and to be of relevance to observation from space, 93 stations were selected for their favorable environmental conditions (clear sky, low winds, and smooth water surfaces). The sun zenith angle values range between 30° and 80° for these selected stations (with a mean value of 51° and a standard deviation of ±16°). These measurements were corrected for errors due to the instrument self-shading, calculated as prescribed by *Leathers and Downes* [2004].

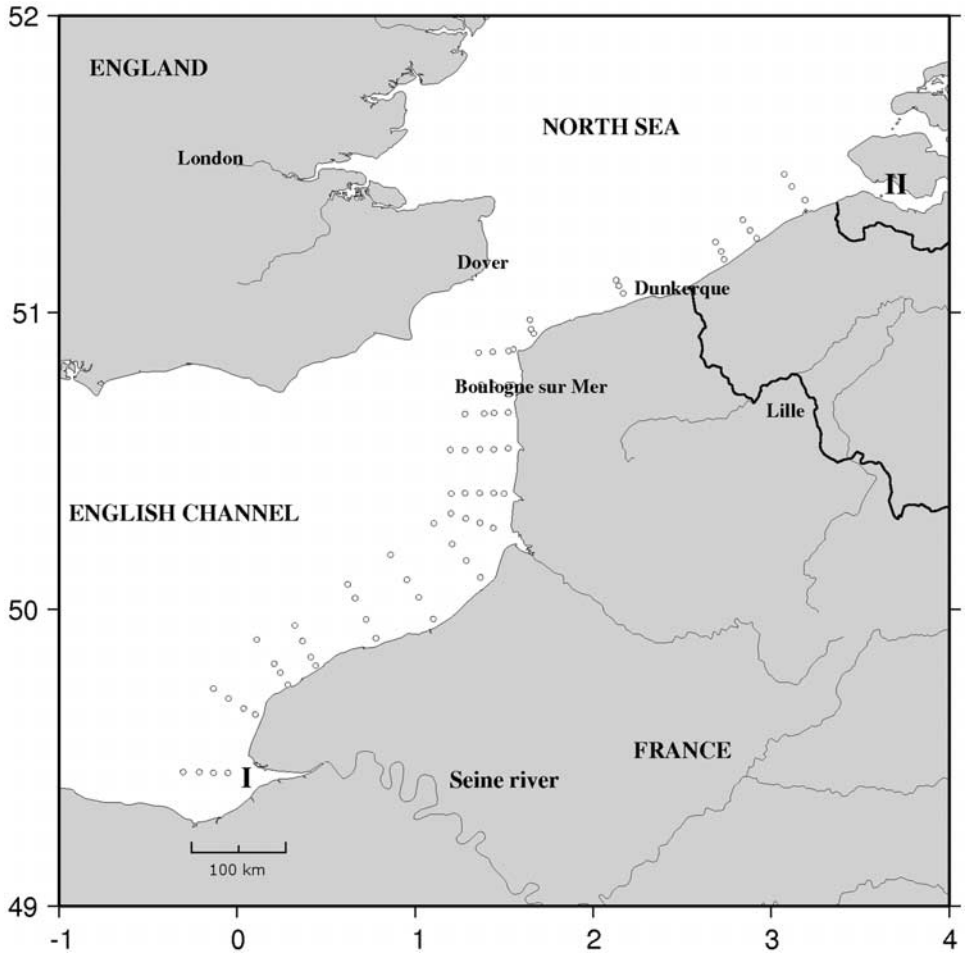

Figure 1. Location of the different stations visited in March (15–18), April (11–16), May (10–15), and June (25–30) 2004. The investigated area is bordered by (a) the mouth of the Seine river in the south and (b) the mouth of the Escault river in the North.

2.3. Optical Parameters and Discrete Water Samples

[9] Simultaneously with the radiometric measurements, a set of subsurface water samples was collected at each station as well as optical parameters. The different biogeochemical and optical measured parameters include chlorophyll *a* concentration (*Chl*), absorption by colored dissolved organic matter ($a_{\mathrm{CDOM}}(\lambda)$), and particulate scattering and backscattering coefficients at 650 nm ($b_{\mathrm{p}}(650)$ and $b_{\mathrm{bp}}(650)$, respectively). In situ optical parameters were measured from an optical package (WET Labs, Inc.) including a chlorophyll fluorometer, a 10 cm path length beam transmissiometer (at wavelength λ = 650 nm), and a backscatter sensor (at 650 nm, WET Labs ECO-VSF), which measures the optical scattering at three distinct angles: 100, 125, and 150 degrees. The methods used to get $b_{\mathrm{p}}(650)$ and $b_{\mathrm{bp}}(650)$ from the beam transmissometer and the ECO-VSF, respectively, are described by *Loisel et al.* [2007]. Measurements of *Chl* were performed from particulate matter collected on glass fiber filters (Whatman, GF/F), as described by *Loisel et al.* [2007]. To determine $a_{\mathrm{CDOM}}(\lambda)$, seawater samples were filtered on 0.22-μm Millipore membrane. Absorbance of the filtrates was then measured in a 10-cm quartz cuvette at 1 nm resolution between 350 and 750 nm using a dual beam spectrophotometer. The mean value of the interval 680–690 nm was subtracted from the spectrum (baseline correction, *Babin et al.* [2003a]) and the absorbance was then converted into an absorption coefficient. The spectral slope (S_{CDOM}) was calculated using a nonlinear exponential fit function on the 350–500 nm spectral range [*Babin et al.*, 2003a]:

$$a_{CDOM}(\lambda) = a_{CDOM}(443) \cdot \exp(-S_{CDOM}(\lambda - 443)) \qquad (2)$$

[10] Algal population enumeration by microscopy is time consuming and labor intensive. Therefore this enumeration was performed only on preselected stations based on the classification of the $R_{\mathrm{rs}}(\lambda)$ spectra defined by *Lubac and Loisel* [2007]. Fifteen stations were selected to encompass waters where the phytoplankton community was mixed or dominated by either *P. globosa* or diatoms. Five stations were chosen from the class 1 and class 4 of *Lubac and Loisel* [2007], which are associated with dominance of the algal community by *P. globosa* and diatoms, respectively. Five stations were chosen from the class 3 of *Lubac and Loisel* [2007], which is considered as an intermediate class between the two previous. For each station, a seawater volume of 250 mL was preserved immediately with Lugol's solution for phytoplankton analysis. Cell counting was performed under inverted microscopy (Nikon TE2000-S) according to the Utermöhl method (1958). Cells sizes and shapes were examined with a camera (Nikon DS5M) and measurements were performed with specific software

(Nikon NIS element). Individual volumes and surface areas of each phytoplankton cell were estimated by assuming simple geometric forms [*Sun and Liu*, 2003]. Diatom carbon biomass was calculated on the basis cell concentration and volume-specific cell carbon content [*Menden-Deuer and Lessard*, 2000]. Only solitary stages of *P. globosa* (flagellates and colonial cells) were identified in the samples, because *P. globosa* colonies are disrupted by fixation. The carbon biomass of *P. globosa* solitary cells was estimated using cell concentration and a correction factor [*Edler*, 1979; *Van Rijssel et al.*, 1997; *Schoemann et al.*, 2005].

2.4. Derivative Analysis

[11] Derivative spectroscopy is commonly used in the analysis of hyperspectral remote sensing reflectance data [*Dick and Miller*, 1991; *Philpot*, 1991; *Chen and Curran*, 1992; *Louchard et al.*, 2002]. Derivatives of second order or higher are relatively less sensitive to variations in illumination intensity, as well as spectral variations of sunlight and skylight [*Tsai and Philpot*, 1998]. The derivative analysis, which amplifies spectral inflections and enhances detection of small spectral variations, is used to closely examine the spectral reflectance patterns. This technique provides information regarding the convexity and concavity of a given reflectance spectrum. In this study, we examine the second derivative of $R_{rs}(\lambda)$ ($d\lambda^2 R_{rs}$) to indicate the center of the secondary peak and trough of $R_{rs}(\lambda)$. $d\lambda^2 R_{rs}$ is estimated using a "finite difference approximation" as:

$$\frac{d^2 R_{rs}}{d\lambda^2}|i \cong \frac{R_{rs}(\lambda_{i+1}) - 2R_{rs}(\lambda_i) + R_{rs}(\lambda_{I-1})}{(\Delta\lambda)^2} \quad (3)$$

where the finite band resolution $\Delta\lambda = \lambda_i - \lambda_{i+1}$ is 2.5 nm. Derivatives are very sensitive to noise in hyperspectral analysis. In order to minimize random noise, a running average filter is applied locally to smooth data prior to the derivative analysis. The algorithm is given by:

$$\overline{R}_{rs}(\lambda_i) = \frac{\sum_{j=1}^{n} R_{rs}(\lambda_j)}{n} \quad (4)$$

where n is the filter size (here $n = 5$) and i is the index of the middle point of the filter.

2.5. Similarity Index Analysis

[12] This analysis was introduced in phytoplankton ecology by *Millie et al.* [1997] and *Kirkpatrick et al.* [2000] to compare the fourth derivative of measured phytoplankton absorption spectra with that of a known phytoplankton absorption spectrum for identification purposes. SI is determined by computing the angle between two spectra, considered here as vectors:

$$SI = 1 - \left(\frac{2}{\pi} \times \arccos\left(\frac{A_{ref} \cdot A_{unk}}{|A_{ref}| \times |A_{unk}|}\right)\right) \quad (5)$$

where A_{ref} is the reference vector that encompasses the fourth derivative of a given phytoplankton population absorption spectrum obtained from laboratory cultures, and A_{unk} is similar to A_{ref}, but for an unknown phytoplankton population. SI varies linearly between zero and one. Zero indicates no similarity between the reference and the unknown vectors, one indicates complete similarity between the reference and the unknown vectors.

2.6. Sensitivity Analysis

[13] To detect *P. globosa* blooms with multispectral remote sensors, we use two ratios of $R_{\mathrm{rs}}(\lambda)$ taken in the visible part of the spectrum. Because $R_{\mathrm{rs}}(\lambda)$ is sensitive to other optically significant components than phytoplankton, a sensitivity analysis has to be performed to evaluate their impacts on the $R_{\mathrm{rs}}(\lambda)$ ratios. We specifically test the effects of *Chl*, *CDOM*, and the composition of the particulate matter (through the $b_{\mathrm{bp}}(650)$ to $b_{\mathrm{p}}(650)$ ratio, $b_{\mathrm{bp}}/b_{\mathrm{p}}$) on the two $R_{\mathrm{rs}}(\lambda)$ ratios. *Chl* is selected as a variable parameter to examine the effect of the intensity of the bloom on these ratios. *CDOM* is chosen because its absorption at low wavelengths may dominate the phytoplankton absorption. Finally, $b_{\mathrm{bp}}/b_{\mathrm{p}}$ is selected because of its fundamental role in the ocean color variability in coastal waters [*Lubac and Loisel*, 2007]. The Hydrolight radiative transfer model (Hydrolight 4.2 [*Mobley and Sundman*, 2001]), which computes radiances distributions in the ocean, is employed to conduct the sensitivity analysis. The simulations are run for a nearly flat sea surface with a wind speed fixed at 5 m s^{-1}, a sun zenith angle at 50° corresponding to the mean sun angle observed at the 15 selected stations, and an infinitely deep ocean (no bottom reflection for the investigated waters). The inherent optical properties fixed as input parameters for the simulations are given below.

[14] A model with three components (seawater, particles, and *CDOM*) is used to calculate the values of the absorption ($a(\lambda)$) and backscattering ($b_{\mathrm{b}}(\lambda)$) coefficients for variable *Chl*, *CDOM*, and $b_{\mathrm{bp}}/b_{\mathrm{p}}$ values. The backscattering and absorption spectra are partitioned as follows:

$$b_{\mathrm{b}}(\lambda) = b_{\mathrm{bw}}(\lambda) + b_{\mathrm{bp}}(\lambda) \quad (6)$$

$$a(\lambda) = a_{\mathrm{w}}(\lambda) + a_{\phi}(\lambda) + a_{\mathrm{CDOM}}(\lambda) \quad (7)$$

where $b_{\mathrm{bw}}(\lambda)$ and $a_{\mathrm{w}}(\lambda)$ are the pure seawater backscattering and absorption coefficients, respectively. $b_{\mathrm{bp}}(\lambda)$ is the particulate backscattering coefficient, and $a_{\phi}(\lambda)$ and $a_{\mathrm{CDOM}}(\lambda)$ are the phytoplankton and dissolved absorption coefficients, respectively. The nonalgal particles represent less than 10% of the total absorption during the spring-summer period of the investigated waters [*Vantrepotte et al.*, 2007]. In addition, the absorption of the nonalgal particles ($a_{\mathrm{nap}}(\lambda)$) has a spectral shape similar to $a_{\mathrm{CDOM}}(\lambda)$, and is therefore not included in this sensitivity analysis. The values of $a_{\mathrm{w}}(\lambda)$ and $b_{\mathrm{bw}}(\lambda)$ are given by *Pope and Fry* [1997] and *Morel* [1974], respectively. The nonwater IOP spectra are then parameterized as:

$$\begin{aligned} a_{\phi}(\lambda) &= Chl.a^{*}_{\phi}(\lambda), \text{ with } a^{*}_{\phi}(\lambda) \\ &= (1-w).a^{*}_{phaeo}(\lambda) + w.a^{*}_{diato}(\lambda) \end{aligned} \quad (8)$$

$$a_{\mathrm{CDOM}}(\lambda) = a_{\mathrm{CDOM}}(443).\exp(-S_{\mathrm{CDOM}}(\lambda - 443)) \quad (9)$$

$$b_{\mathrm{bp}}(\lambda) = b_{\mathrm{bp}}/b_{\mathrm{p}}.Chl.b^{*}_{\mathrm{p}}(\lambda), \text{with } b^{*}_{\mathrm{p}}(\lambda) = b^{*}_{\mathrm{p}}(650).(650/\lambda)^{v} \quad (10)$$

Table 1. Values Adopted for the Different Parameters Used in Each Scenario of the Sensitivity Analysis[a]

	Chl, mg·m^{-3}	b_{bp}/b_p	$a_{CDOM}(443)$, m^{-1}
Scenario I	[5;30]	= 0.006	= 0.15
Scenario II	= 10	[0.003;0.03]	= 0.15
Scenario III	= 10	= 0.006	[10% of $a(443)$; 60% of $a(443)$]

[a]Note that for each scenario, S_{CDOM} is fixed at 0.016 nm^{-1}, and the w parameter takes successively the 0.0, 0.5, and 1.0 value.

where $a^*_{phaeo}(\lambda)$, and $a^*_{diato}(\lambda)$ are the chlorophyll specific absorption of *P. globosa* and diatoms, respectively. Their spectral values were obtained from measurements performed on cultures [*Astoreca*, 2007]. The specific absorption weighting factor (w) varies from 0 to 1. This parameter represents the relative concentration in terms of chlorophyll associated with each phytoplankton and allows the simulation of an algal community either mixed or dominated by *P. globosa* or diatoms. The values of the *CDOM* spectral slope (S_{CDOM}) and of $b^*_p(650)$ (= $b_p(650)/Chl$) are chosen to be 0.016 nm^{-1}, and 0.14 m^2 mg^{-1}, respectively. These values are based on our in situ measurements performed during bloom conditions. The spectral dependence (ν) of $b^*_p(\lambda)$ is fixed at 0.5 [*Babin et al.*, 2003b]. This value is also in good agreement with in situ measurements reported by *Loisel et al.* [2006] for *Chl* values greater than 10 mg.m^{-3} (see their Figure 7b).

[15] Three computational scenarios, in which *Chl*, b_{bp}/b_p, and $a_{CDOM}(443)$ vary independently, are examined (see Table 1). For each scenario, w successively takes a value of 0.0, 0.5, or 1.0 to simulate an algal population dominated by *P. globosa*, mixed, or dominated by diatoms, respectively. In scenario I, b_{bp}/b_p and $a_{CDOM}(443)$ are held at 0.006 and 0.15 m^{-1}, respectively. These values correspond to the mean values observed during *P. globosa* and diatoms bloom conditions. Note that the extreme values of b_{bp}/b_p (higher than 0.019) are not taken into account in the calculation of the mean (these values are associated with particular conditions during which the nonalgal or mineral particulate fractions are particularly high). *Chl* varies from 5 to 30 mg·m^{-3}. In scenario II, $a_{CDOM}(443)$ and *Chl* are held at 0.15 m^{-1} and 10 mg·m^{-3}, respectively. b_{bp}/b_p is allowed to vary from 0.003 to 0.03. This range of b_{bp}/b_p values is intended to encompass both realistic ranges observed in the field and extreme values. In scenario III, b_{bp}/b_p and *Chl* are fixed at 0.006 and 10 mg·m^{-3}, respectively, while *CDOM* varies from 10 to 60% of $a(443)$, as observed by *Vantrepotte et al.* [2007].

3. Results

3.1. $R_{rs}(\lambda)$ Spectra and Enumeration Results

[16] Figure 2a shows the $R_{rs}(\lambda)$ spectra collected during the 4 cruises occurring in March, April, May, and June 2004. The $R_{rs}(\lambda)$ spectra display great variability in both magnitude and spectral shape. This is directly related to the various and largely uncorrelated constituents that are suspended or dissolved in the waters, and for which the relative concentrations change according to different biological (blooms formation, and degradation) and physical (resuspension, dilution, and aggregation) processes. This variability is analyzed by *Lubac and Loisel* [2007]. They stressed that the variability of the $R_{rs}(\lambda)$ spectra are, to first order, related to variability in particulate backscattering, and, to second order, by absorption associated with *CDOM* and detritus. They also highlighted the role of the bulk particulate composition, through b_{bp}/b_p, in the $R_{rs}(\lambda)$ variability. The variability of the spectral shape of $R_{rs}(\lambda)$ was related to the characteristics of the water constituents from a hierarchical cluster analysis. In particular, they showed that the $R_{rs}(\lambda)$ spectra associated with phytoplankton (*P. globosa* and diatoms) blooms may be discerned from the others. Figure 2b shows the $R_{rs}(\lambda)$ spectra associated with the 15 stations preselected for the enumeration of the phytoplankton species. The spectral shape of these $R_{rs}(\lambda)$ spectra is typical of a phytoplankton bloom situation with low values in the blue and high values in the green. The chlorophyll *a* (*chl-a*) absorption peak at 660 nm and the *chl-a* fluorescence peak at 683 nm can clearly be discerned on the $R_{rs}(\lambda)$ spectra. The high variability of the $R_{rs}(\lambda)$ magnitude in the green part of the spectrum may be directly related to the variability of the b_{bp}/b_p ratio values, which range from 0.005 to 0.021 (Table 2).

[17] The results of the laboratory-based cell enumeration are displayed in Table 2. The abundance of *P. globosa* varies from 0 to 33.451 10^6 cells·l^{-1}, while the diatoms abundance varies from 0.555 to 2.197 10^6 cells·l^{-1}. These high values of abundance highlight the extreme intensity of the *P. globosa* and diatoms blooms, whose the bloom condition threshold values are typically found to be around 10^6 and 10^5 cells·l^{-1}, respectively [*Cadée*, 1992; *Schoemann et al.*, 2005]. Here, the biomass of the algal population is considered as the sum of the biomass of *P. globosa* (C_p) and diatoms (C_d), which greatly dominates the algal community from March to June (from ~80 to 90% according to *Vantrepotte et al.* [2007]). *P. globosa* biomass ranged from 0 to 83% while diatoms biomass ranged from 17 to 100%. Note that diatoms are dominated by *Guinardia delicatula* and *Rhizosolenia imbricate*. From these laboratory-based cell enumerations, three groups may be discerned. While group 1 and group 3 correspond to an algal population dominated by *P. globosa* ($C_p > 60\%$ and $C_d < 40\%$) and diatoms ($C_d > 90\%$ and $C_p < 10\%$), respectively, group 2 is associated with a mixed algal community ($40\% < C_p < 60\%$).

3.2. Hyperspectral Analysis

[18] Figure 3 shows the mean absorption spectra and their second derivatives of *P. globosa* and diatoms measured by *Astoreca* [2007] from cultures. Note that the diatoms species used in the cultures correspond to those observed in situ. The spectral shape of the two absorption spectra and their second derivatives differ mainly in the 400–540 nm spectral domain. The main differences between the second derivatives of the two phytoplankton absorption spectra are the position of the minimum within 460–470 nm and of the maximum within 480–500 nm. Whereas the minimum is observed at 465 nm for diatoms, it is observed at 469 nm for *P. globosa*. Likewise, while the maximum is observed at 483 nm for diatoms, it is observed at 493 nm for *P. globosa*. Figure 4a shows the $R_{rs}(\lambda)$ mean spectra of group 1, group 2, and group 3, which are characteristic of a *P. globosa* bloom situation, mixed algal population, and a diatoms

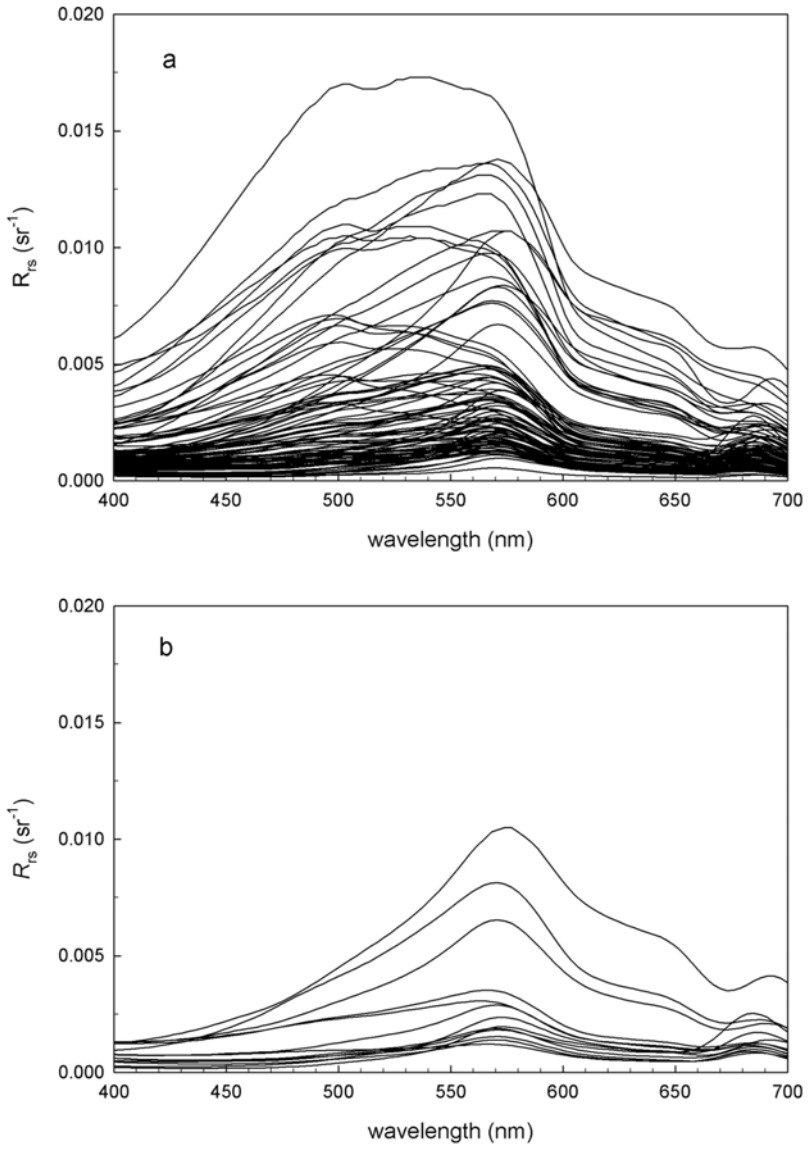

Figure 2. (a) Hyperspectral measurements of $R_{rs}(\lambda)$ spectra (N = 93) obtained from field radiometric measurements performed in the eastern English Channel and southern North Sea from March to June 2004. (b) $R_{rs}(\lambda)$ spectra (N = 15) measured at the stations selected for the enumeration of the phytoplankton species.

bloom situation, respectively. Figure 4b shows the second derivative of the mean $R_{rs}(\lambda)$ spectrum of each group in the 400–540 nm spectral domain. A positive maximum in the second derivative of $R_{rs}(\lambda)$ corresponds to an inflexion point in the $R_{rs}(\lambda)$ spectra. Because $R_{rs}(\lambda)$ is inversely proportional to $a(\lambda)$, a minimum (maximum) in the reflectance spectrum corresponds to a maximum (minimum) in the absorption spectrum. The shifts observed in Figure 3b for the second derivative of the phytoplankton absorption spectra are also observed on the second derivatives of $R_{rs}(\lambda)$. The labeled diatoms and *P. globosa* $R_{rs}(\lambda)$ second derivative spectra are characterized by maxima around 462.5 and 472.5 nm, respectively. At 482.5 and 500 nm, minima are observed for the diatoms and *P. globosa* $R_{rs}(\lambda)$ second derivative spectra, respectively. Note that the minimum of the second derivative of $R_{rs}(\lambda)$ (at 500 nm) for *P. globosa* is significantly shifted in comparison to the maximum of the second derivative of $a_\phi(\lambda)$ (at 493 nm) obtained from cultures (see discussion).

[19] To characterize these shifts, the relationships between the proportion of the biomass of *P. globosa* (in %) and the position of the maximum and minimum of the $R_{rs}(\lambda)$ second derivative in the 460–480 nm and 480–510 nm spectral domain, respectively, are displayed in Figure 5. Figure 5a shows a significant relationship between the biomass of *P. globosa* and the position of the maximum (r^2 = 0.92). This indicates that the maximum is around 462.5 nm for a C_p close to 0% ($C_d \sim 100\%$) and around 475 nm for a C_p value close to 90%. Similarly, a good linear relationship is observed (r^2 = 0.95) between C_p and the position of the minimum of the $R_{rs}(\lambda)$ second derivative in the 480–510 nm spectral range (Figure 5b). When the C_p value is close to 0%, the minimum value of

Table 2. Chlorophyll *a* Concentration (*Chl*, mg·m^{-3}), Backscattering Ratio (b_{bp}/b_p), Abundance (N, 10^6 cell·l^{-1}) and Biomass (C_i, %) of *P. globosa* and Diatoms Measured for Each Selected Station

					P. globosa		Diatoms	
Group	Station	Month	*Chl*, mg·m^{-3}	b_{bp}/b_p	N (10^6 cells·l^{-1})	C_p (%)	N (10^6 cells·l)	C_d (%)
1	33	5	33.3	0.005	33.451	77	1.303	23
1	37	5	20	0.005	21.982	83	0.896	17
1	38	5	17.6	0.005	15.489	66	0.954	34
1	39	5	17.2	0.005	18.296	81	0.731	19
1	50	5	9.4	0.009	8.157	71	0.463	29
1	64	4	20	0.007	18.322	64	2.197	36
1	65	4	9.2	0.020	14.803	60	1.563	32
2	38	4	10.4	0.010	2.024	40	0.569	60
2	42	4	12.2	0.006	4.272	41	0.702	59
2	56	4	10	0.019	6.175	55	0.555	45
3	9	6	4.1	0.005	0	0	1.443	100
3	28	6	7.0	0.007	0.084	5	1.505	95
3	38	6	7.8	0.019	0.057	5	1.051	95
3	42	6	8.7	0.021	0.039	2	1.142	98
3	15	5	11.5	0.006	0.028	2	1.094	98

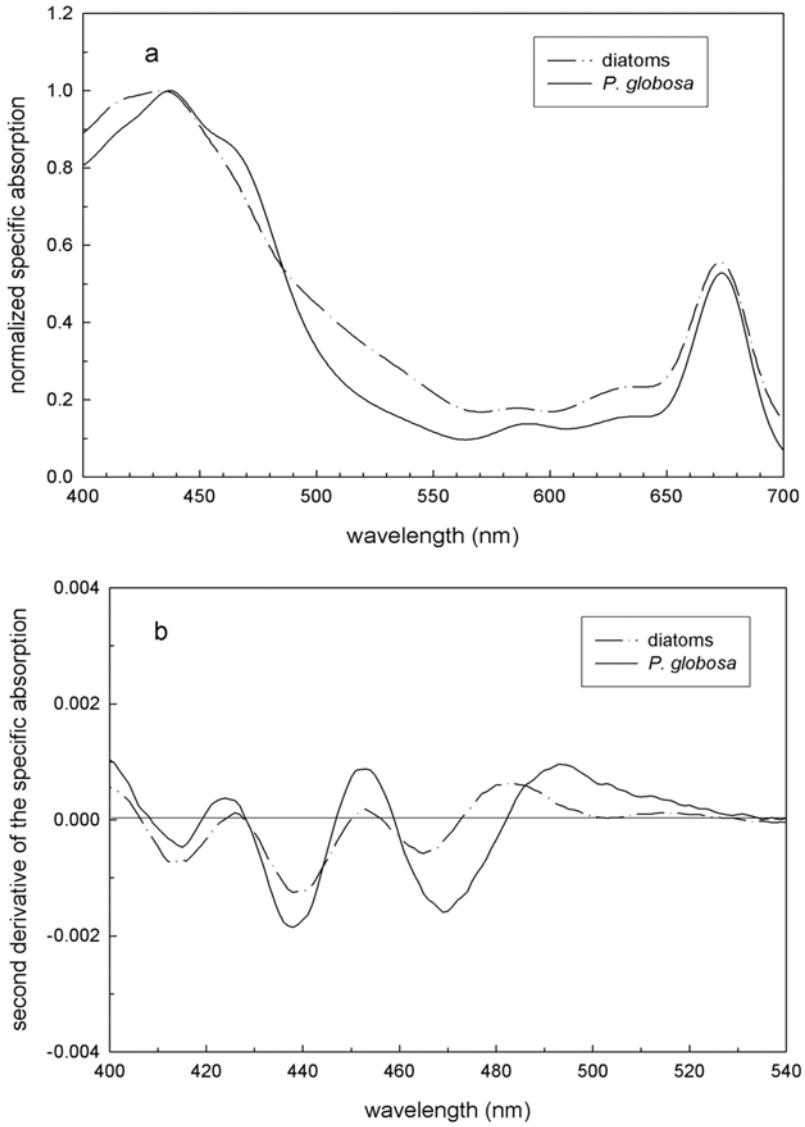

Figure 3. (a) Normalized diatoms and prymnesiophyceae *P. globosa* absorption spectra obtained from cultures and (b) their second derivatives (redrawn from *Astoreca* [2007]). The normalization is performed using the absorption value of each spectrum at 442 nm.

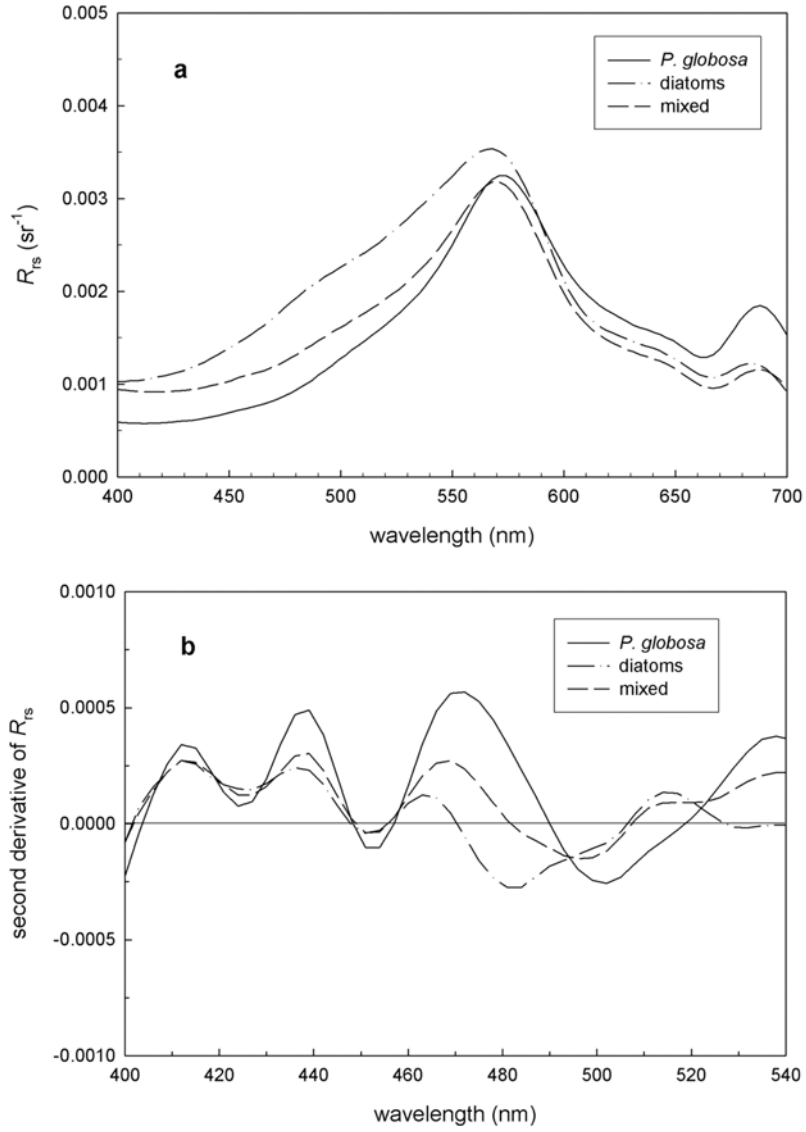

Figure 4. (a) Mean and (b) second derivatives spectra of $R_{rs}(\lambda)$ associated with the group 1 (*P. globosa*), group 2 (mixed), and group 3 (diatoms) (see Table 1).

$d\lambda^2 R_{rs}$ is observed around 480 nm, and when C_p tends toward 90%, this minimum is observed around 510 nm.

[20] The method based on the shifts of the extremes in the $d\lambda^2 R_{rs}$ spectra is chosen to identify the spectra corresponding to a *P. globosa* bloom in our whole $R_{rs}(\lambda)$ data set. On the basis of the results presented above, we define two criteria to discriminate the *P. globosa* blooms from diatoms blooms (C_p higher than 60%): the maximum of $d\lambda^2 R_{rs}$ in the 460–480 nm spectral range has to be observed beyond 471 nm, and the minimum of $d\lambda^2 R_{rs}$ in the 480–510 nm spectral range has to be observed beyond 499 nm. The application of these two criteria to our whole $R_{rs}(\lambda)$ data set provides 21 spectra associated with *P. globosa* blooms. This is in agreement with a qualitative analysis based on our in situ observations.

3.3. Comparison of the $R_{RS}(\lambda)$-Hyperspectral Analysis With the $a_\phi(\lambda)$-Similarity Index Analysis

[21] The classification of the $R_{rs}(\lambda)$ spectra obtained from the two criteria presented above, is compared to that achieved by means of a similarity index analysis as described by *Millie et al.* [1997]. This last method was successfully applied for the detection and assessment of the harmful alga, *Karenia Brevis* [*Craig et al.*, 2006]. In the present study, the similarity index (SI) is computed between the second derivative of an in situ reference *P. globosa* absorption spectrum ($a^{ref}_{phaeo\text{-}in\ situ}(\lambda)$) and the second derivative of an in situ unknown phytoplankton population absorption spectrum ($a_{\phi\text{-}in\ situ}(\lambda)$) in the 400–540 nm spectral range. Then, based on a relationship between SI and the *P. globosa* biomass, the absorption spectra identified as *P. globosa* are selected. This study is performed in 400–540 nm spectral range because, the spectral variability of $a_\phi(\lambda)$ is sufficiently high to discriminate a phytoplankton community dominated by *P. globosa* from a phytoplankton community dominated by diatoms. Indeed, the SI value computed between the second derivative of the *P. globosa* absorption spectrum and the second derivative of the diatoms absorption spectrum, both obtained from culture,

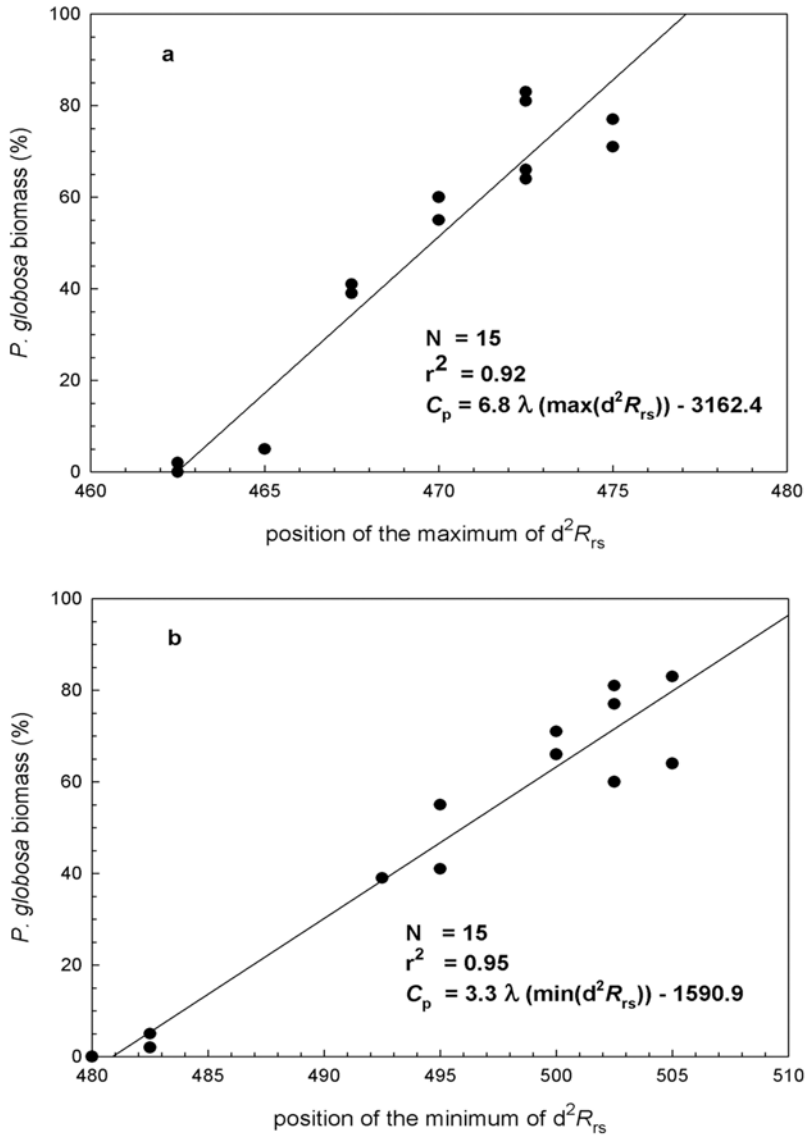

Figure 5. Variation of the *P. globosa* biomass (C_p, expressed in %) as a function of (a) the position of the maximum of the second derivative of $R_{rs}(\lambda)$ in the range 460–480 nm ($\lambda(\max(d^2R_{rs}))$), and (b) the position of the minimum of the second derivative of $R_{rs}(\lambda)$ in the range 480–510 nm ($\lambda(\min(d^2R_{rs}))$). The black lines represent the linear regressions between Figure 5a C_p and $\lambda(\max(d^2R_{rs}))$, and Figure 5b C_p and $\lambda(\min(d^2R_{rs}))$. The regression equations, the number of observations (N), and the squared correlation coefficient (r^2) are given.

is around 0.59 in the 400–540 nm spectral range, versus 0.78 in the 400–700 nm spectral range.

[22] Because of the lack of in situ phytoplankton absorption measurements, $a_{\phi\text{-in situ}}(\lambda)$ is derived from $R_{rs}(\lambda)$ using the quasi-analytical algorithm of *Lee et al.* [2002]. Figure 6a shows the spectra of $a_\phi(\lambda)$ retrieved from our whole $R_{rs}(\lambda)$ data set. $a^{ref}_{\text{phaeo-in situ}}(\lambda)$ is then computed as the mean spectrum of the retrieved $a_{\phi\text{-in situ}}(\lambda)$ associated with *P. globosa* blooms (group 1 in Table 2). To verify the consistency of the retrieval, the spectrum of $a^{ref}_{\text{phaeo-in situ}}(\lambda)$ and its second derivative are compared to those obtained from *P. globosa* cultures by *Astoreca* [2007], ($a_{\text{phaeo-culture}}(\lambda)$) (Figures 6b–6c). A relatively good agreement is observed between the field retrieved and laboratory measured absorption spectra (Figure 6b). Importantly, the maxima and minima of the second derivative of $a^{ref}_{\text{phaeo-in situ}}(\lambda)$ and $a_{\text{phaeo-culture}}(\lambda)$ are observed at the same wavelengths (Figure 6c). The main sources of discrepancies between the

Figure 6. (a) Phytoplankton absorption spectra (N = 93) retrieved from $R_{rs}(\lambda)$ using the quasi-analytical algorithm developed by *Lee et al.* [2002]. (b) Field retrieved ($a^{ref}_{\text{phaeo-in situ}}(\lambda)$) and laboratory measured ($a_{\text{phaeo-culture}}(\lambda)$) normalized absorption spectra of *P. globosa* (see text for details), and (c) their second derivatives.

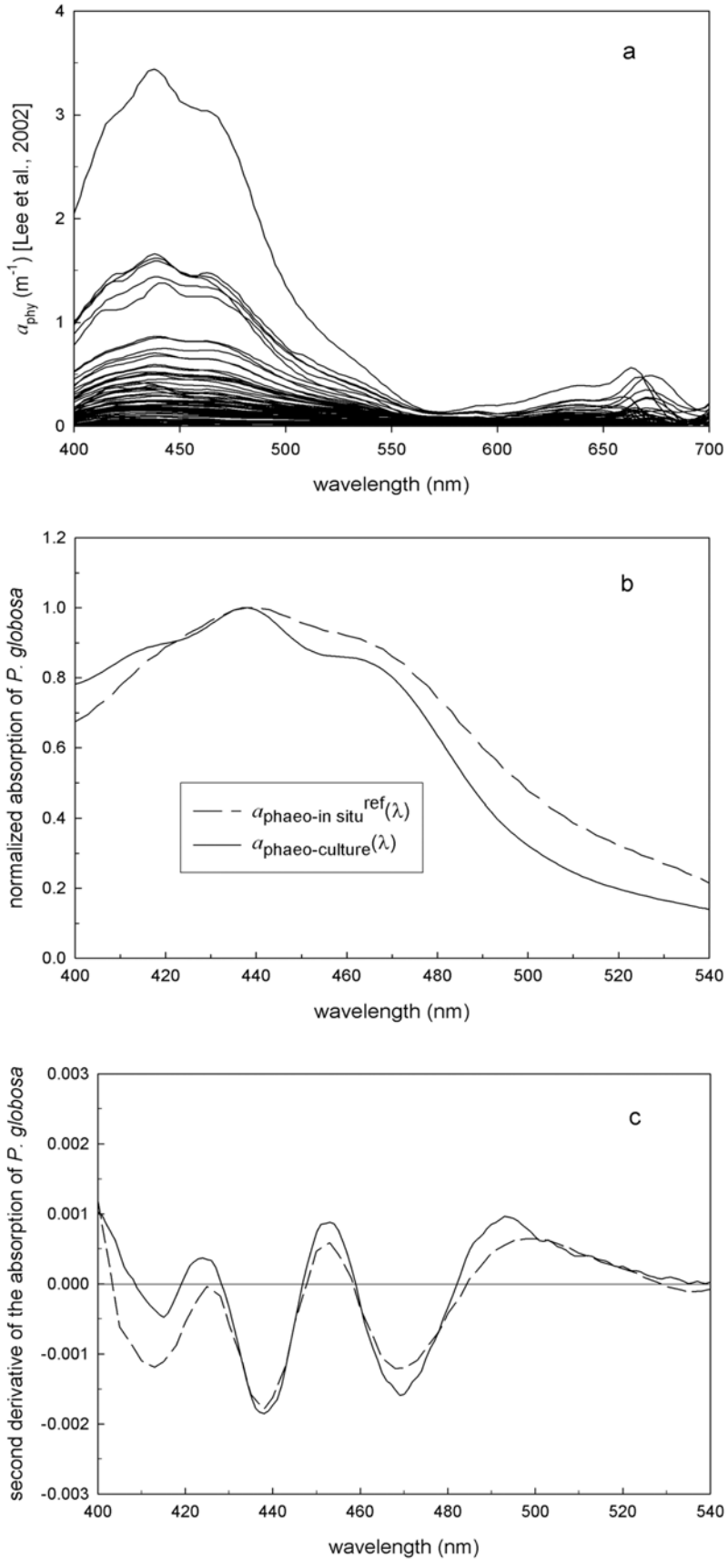
a
a_{phy} (m^{-1}) [Lee et al., 2002]
wavelength (nm)
b
normalized absorption of P. globosa
$a_{phaeo\text{-}in\ situ}^{ref}(\lambda)$
$a_{phaeo\text{-}culture}(\lambda)$
wavelength (nm)
c
second derivative of the absorption of P. globosa
wavelength (nm)

Figure 6

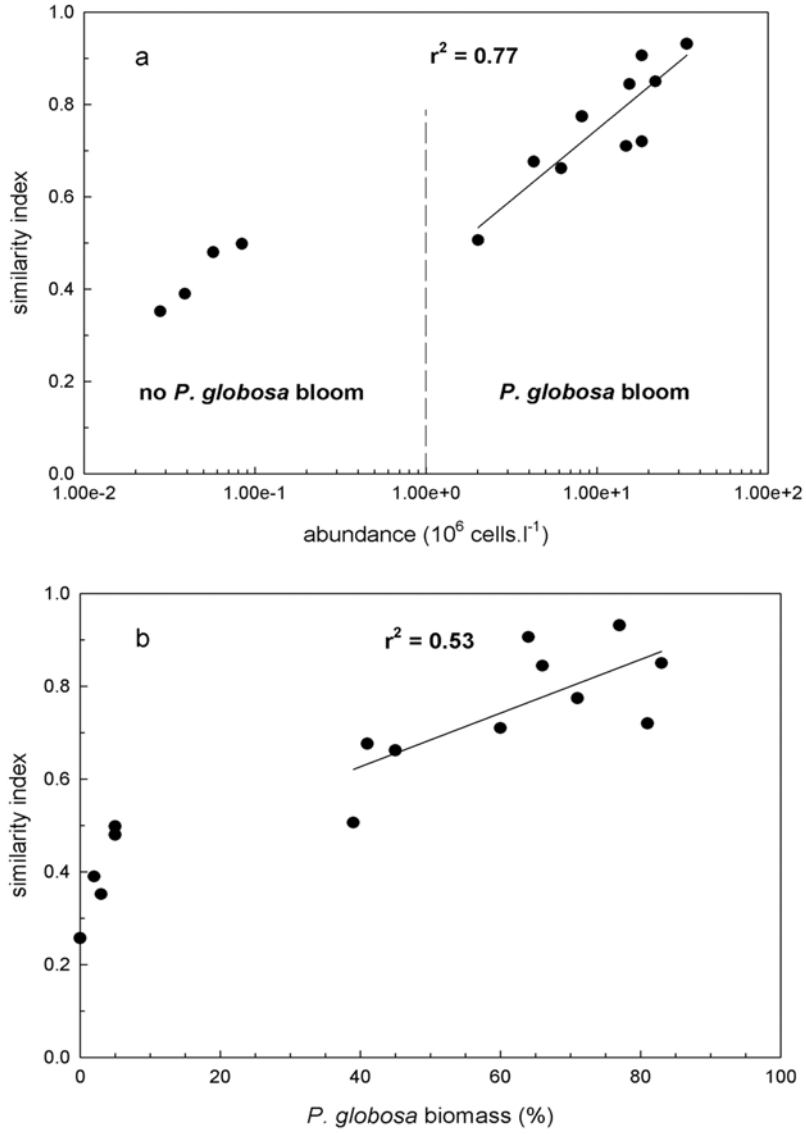

Figure 7. (a) Similarity index magnitude as a function of the *P. globosa* cell abundance. The dashed line represents the separation between a bloom and a no bloom situation. (b) Similarity index magnitude as a function of the *P. globosa* biomass. The squared correlation coefficients (r^2) are calculated for the 10 points associated with a bloom situation.

two spectra are due to the errors in the retrieval of $a_{\phi\text{-in situ}}(\lambda)$ from $R_{rs}(\lambda)$, owing to the assumptions and empirical relationships used in the quasi-analytical algorithm; but also to the cell properties which differ whether they grew in culture or in the field.

[23] Figure 7a shows the relationship between the abundance (in 10^6 cells·l^{-1}) and the similarity index of *P. globosa*. For the 10 points associated with a *P. globosa* bloom, a good correlation between the two parameters is observed ($r^2 = 0.77$). A relatively good correlation ($r^2 = 0.53$) is also observed between the similarity index associated with the 10 points corresponding to a *P. globosa* bloom and the biomass (Figure 7b). The similarity index value of 0.71, associated with a C_p value higher than 60% (and abundance higher than 8.000 10^6 cells·l^{-1}), is then taken to characterize an algal population dominated by *P. globosa*. The similarity index analysis applied to our $R_{rs}(\lambda)$ data set provides 18 spectra associated with a *P. globosa* bloom. The comparison between the results obtained from the position of the maximum and minimum of $d\lambda^2 R_{rs}$ and those obtained from the similarity index analysis to select the stations where *P. globosa* dominates the algal population is displayed in Figure 8. The two methods are in agreement with 17 stations dominated by *P. globosa* identified by both methods (out of 21 for the hyperspectral approach and 18 for the similarity index analysis).

3.4. Multispectral Analysis

[24] Two different empirical approaches were tried to detect the *P. globosa* blooms from multispectral data. The first approach relates the biomass and relative abundance of *P. globossa* with two possible configurations of R_{rs} ratios:

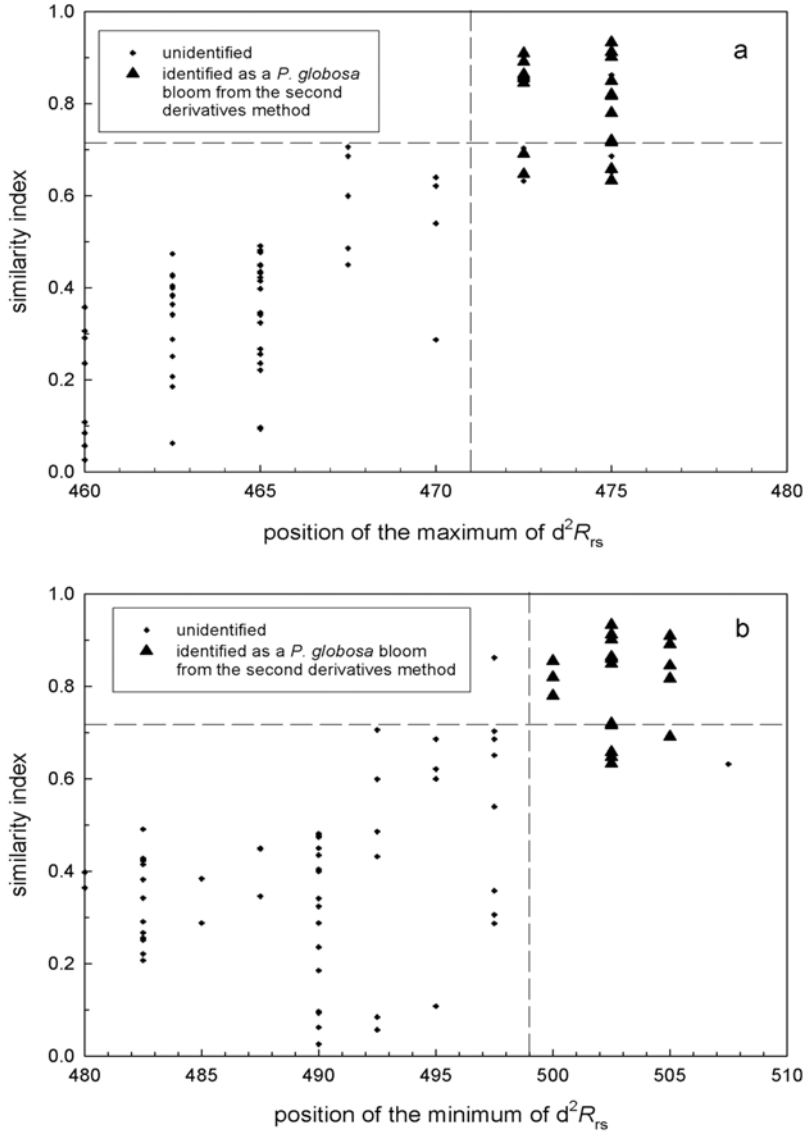

Figure 8. Similarity index magnitude of *P. globosa* as a function of the position of (a) the maximum of the $R_{rs}(\lambda)$ second derivative in the 460–480 nm spectral range, and (b) the position of the minimum of the $R_{rs}(\lambda)$ second derivative in the 480–510 nm spectral range. The horizontal dashed lines (SI = 0.71) represent the limit value above which *P. globosa* blooms are detected from the SI analysis. The vertical dashed lines (at λ = 471 nm in Figure 8a and 499 nm in Figure 8b) represent the wavelengths above which *P. globosa* blooms are detected from the second derivatives method. The stations identified by this method are represented by triangles. Unidentified stations are represented by small dots.

$R_{rs}(\lambda_1)/R_{rs}(\lambda_2)$, and $(R_{rs}(\lambda_1) - R_{rs}(\lambda_2))/R_{rs}(\lambda_3)$, with λ_i between 400 and 700 nm, and a spectral resolution of 2.5 nm. Using this approach we did not find a significant relationship. As an alternative approach, we tested all the possible relationships between different R_{rs} ratios ($R_{rs}(\lambda_1)/R_{rs}(\lambda_2)$). The best combination found to detect the blooms of *P. globosa* uses the two following ratios: $R_{rs}(475)/R_{rs}(505)$ and $R_{rs}(442.5)/R_{rs}(495)$.

[25] To evaluate the potential of current multispectral ocean color sensors for the remote detection of *P. globosa* blooms, we have also tested all possible combinations of R_{rs} ratios from the set of SeaWIFS and MODIS wavelengths (412, 443, 490, 510 (SeaWiFS), 532 (MODIS), 555, and 665 nm). The best combination has been found between the $R_{rs}(490)$ to $R_{rs}(510)$ ratio (R_1) and the $R_{rs}(442.5)$ to $R_{rs}(490)$ ratio (R_2). The R_1 versus R_2 relationship is significantly different (at 90% confidence level) between the *P. globosa* and diatoms plus unidentified data sets (Figure 9). The performance in the use of R_1 and R_2 to discriminate *P. globosa* from diatoms is very similar to that obtained from the $R_{rs}(475)/R_{rs}(505)$ and $R_{rs}(442.5)/R_{rs}(495)$ ratios. A regression analysis (Table 3) shows that the variability of R_1 is mainly ruled by *Chl* ($r^2 = 0.52$), while the variability of R_2 seems to be regulated by b_{bp}/b_p ($r^2 = 0.45$), that is by the nature of the bulk particulate assemblage [*Loisel et al.*, 2007]. As seen, the data points associated with *P. globosa*

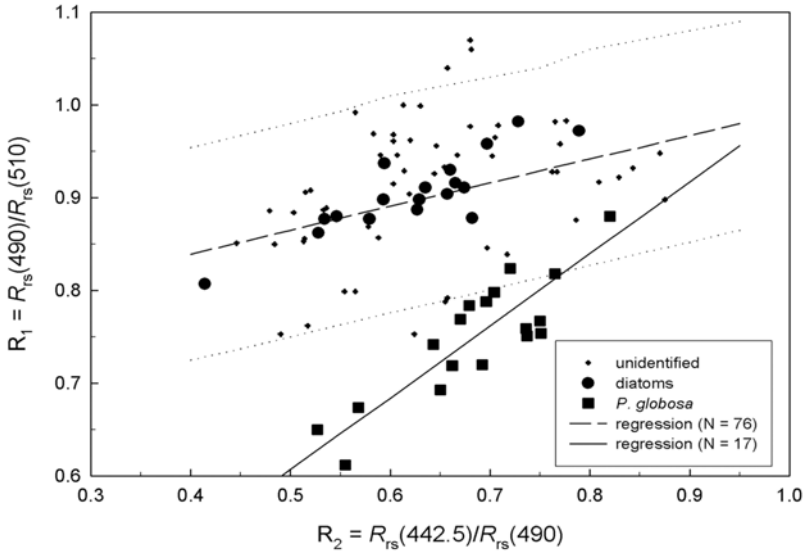

Figure 9. Variation of R_1 as a function of R_2 for the 93 stations selected in this study. The stations identified as dominated by *P. globosa* by the two methods are represented by black squares. The stations identified as dominated by diatoms by a similarity index analysis (results not presented in this article) are represented by solid circles. Unidentified stations are represented by small dots. The curves obtained by least squares fit for *P. globosa* (N = 17) and diatoms plus unidentified stations (N = 76) are represented by the solid and dashed lines, respectively. The dotted lines represent the 90% confidence intervals.

blooms are well separated from those associated with diatoms blooms in the (R_1, R_2) phase space. For a given R_2 value, the stations associated with *P. globosa* show the lowest R_1 values. Given these encouraging results we need to assess if this pattern is really due to the differences in the phytoplankton composition and to evaluate the sensitivity of each ratio to the variation in concentration of the other optically significant components.

[26] Increasing the total chlorophyll concentration and varying the *w* parameter to simulate an algal population dominated by *P. globosa* (w = 0.0), mixed (w = 0.5), and dominated by diatoms (w = 1.0), we find R_1 and R_2 to decrease (Figure 10a). R_1 is more sensitive to the variations of *Chl* than R_2, decreasing twice as fast (0.16 versus 0.8 for a *P. globosa* population) when *Chl* increases from 5 to 30 mg·m^{-3}. R_1 seems more appropriate than R_2 to discriminate waters dominated by *P. globosa* from those dominated by diatoms. Indeed, for a constant *Chl* value, the difference between the R_1 value associated with *P. globosa* and the R_1 value associated with diatoms ($R_1 = R_1|_{w=0} - R_1|_{w=1}$) is greater than 0.2, versus 0.05 for R_2 ($R_2 = R_2|_{w=0} - R_2|_{w=1}$).

[27] For each algal population, when b_{bp}/b_p increases from 0.003 to 0.03, and $a_{CDOM}(443)$ and *Chl* are held constant (scenario II), R_1 and R_2 decrease (Figure 10b). As for scenario I, *P. globosa* and diatoms are very well discriminated from the R_1 ratio. For a constant b_{bp}/b_p value, the R_1 value calculated between the two phytoplankton communities is found to be greater than 0.2, versus 0.05 for R_2. R_2 is more sensitive to the variations of b_{bp}/b_p than R_1. Indeed, when the b_{bp}/b_p ratio increases from 0.004 to 0.03, R_2 decreases more quickly than R_1 for a *P. globosa* population (0.8 versus 0.5). This trend conforms to the results of the correlation analysis performed on our in situ data set (presented in Table 2).

[28] In scenario III, $a_{CDOM}(443)$ varies from 10 to 60% of $a(443)$, while *Chl* and b_{bp}/b_p are held constant. As for scenarios I and II, the R_1 ratio is much more sensitive to the type of phytoplankton (as indicated by the *w* parameter) (Figure 10c). However, this sensitivity decreases as *CDOM* increases. When *CDOM* increases, R_2 decreases for each *w* value, whereas R_1 decreases for a diatoms population, and increases for a mixed and *P. globosa* population. Note that we have also tested the sensitivity of R_1 and R_2 to the spectral shape of *CDOM*, S_{CDOM} (results are not shown). When S_{CDOM} increases from 0.01 to 0.026 nm^{-1}, that is within the range of values observed in situ, R_1 and R_2 decrease for each *w* value, and R_1 stays constant (= 0.22), as for scenarios I and II. This result indicates that S_{CDOM} doesn't affect the discrimination between *P. globosa* and diatoms.

[29] The sensitivity analysis suggests that the composition of the algal community explains much of the behavior of R_1 versus R_2 observed in situ (Figure 9). The discrim-

Table 3. Squared Correlation Coefficient (r^2) Calculated Between R_1 and R_2, and the Discrete In Situ Bio-Optical Parameters, *Chl*, $a_{CDOM}(443)$, $b_p(650)$, b_{bp} (650), and $b_{bp}/b_p(650)$[a]

(N = 93)	R_1	R_2
Chl	**0.52**	0.04
$a_{CDOM}(443)$	0.07	0.08
$b_p(650)$	**0.55**	0.09
$b_{bp}(650)$	0.12	**0.45**
$b_{bp}/b_p(650)$	0.08	**0.44**

[a]The numbers in bold are significant for the null hypothesis at the 99% confidence level.

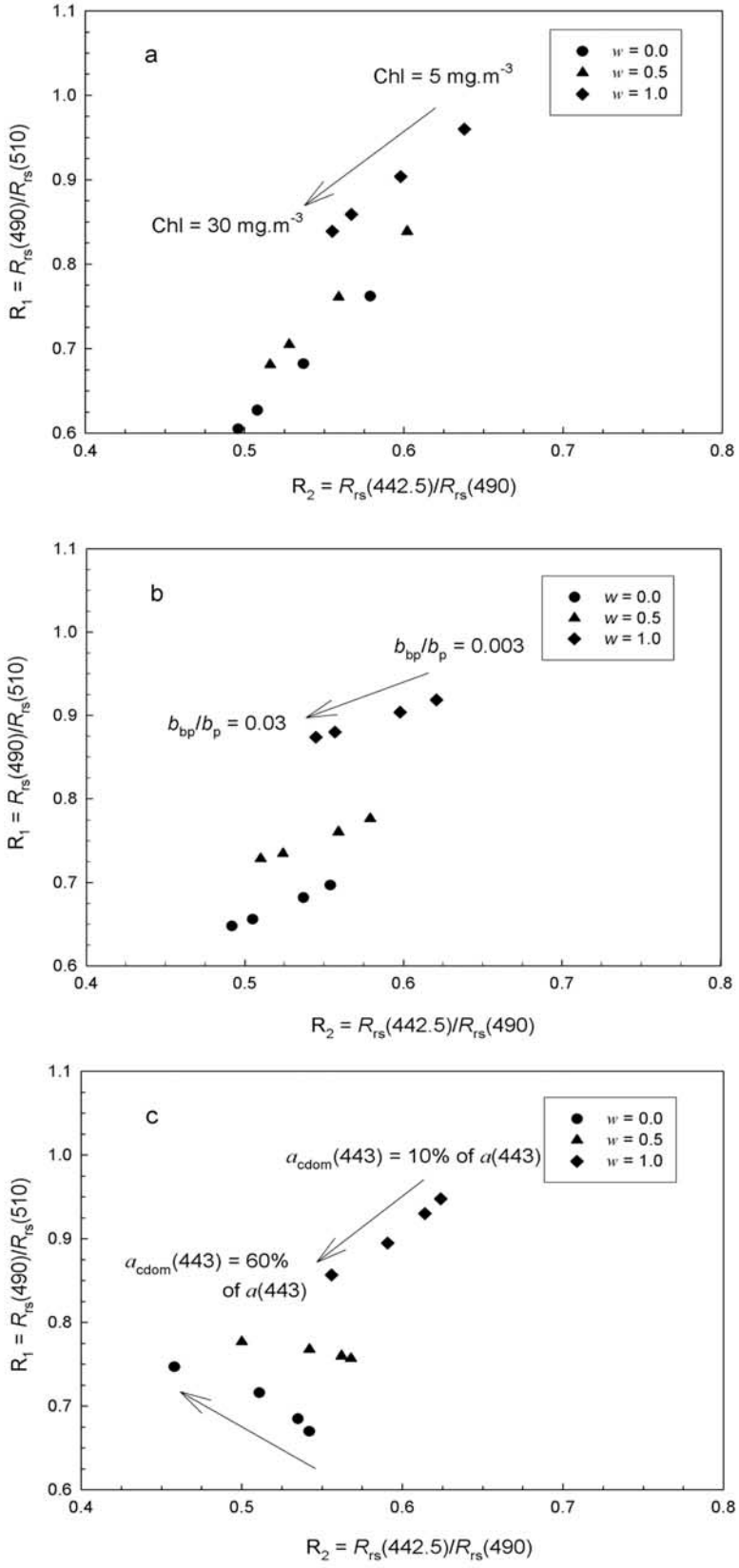
a
w = 0.0
w = 0.5
w = 1.0
Chl = 5 mg.m-3
Chl = 30 mg.m-3
R1 = Rrs(490)/Rrs(510)
R2 = Rrs(442.5)/Rrs(490)
b
bbp/bp = 0.003
bbp/bp = 0.03
c
acdom(443) = 10% of a(443)
acdom(443) = 60% of a(443)

Figure 10

ination between *P. globosa* and diatoms is not significantly affected by the intensity of the bloom (i.e., the *Chl* value), and by the nature of the bulk particulate assemblage (i.e., the b_{bp}/b_p value). The presence of *CDOM* is much more problematic for this discrimination, as the behavior of R_1 with *CDOM* depends on *w*, that is on the phytoplankton assemblage.

4. Discussion and Conclusions

[30] In this paper, we explore the multispectral and hyperspectral approaches to detect *P. globosa* blooms from in situ $R_{rs}(\lambda)$ spectra. The multispectral approach suggests that two reflectance ratios ($R_{rs}(490)/R_{rs}(510)$ and $R_{rs}(442.5)/R_{rs}(490)$) may be used to detect the presence of *P. globosa* blooms from current ocean color sensors. A sensitivity analysis performed on these two ratios shows that *Chl* and b_{bp}/b_p seem to have no effect on the discrimination of a *P. globosa* bloom from a diatoms bloom. In contrast, *CDOM* seems to reduce significantly the ability to distinguish between the two species. Therefore the development of a future remote sensing algorithm, based on the use of these two reflectance ratios, should also include information about *CDOM* (e.g., by including bands in the near-UV, or in situ observations). More radiometric data collected during diatoms and *P. globosa* blooms are needed for the development and validation of such algorithms.

[31] The results of the hyperspectral approach show that *P. globosa* blooms may be distinguished from the second derivative of $R_{rs}(\lambda)$ in the 400–540 nm spectral range. The analysis of $d\lambda^2 R_{rs}$ allows the establishment of two criteria to discriminate *P. globosa* blooms from diatoms blooms. These criteria are based on the position of the maxima (around 471 nm) and minima (around 499 nm) of $d\lambda^2 R_{rs}$, which shift depending on the presence or absence of *P. globosa* blooms. We postulate that these spectral patterns may be directly related to the spectral characteristics of $a_\phi(\lambda)$. Indeed, the *CDOM* and detritus absorption spectra are monotonically decreasing function of wavelength as are the water and particulate backscattering spectra, with the spectral inflexions of the water absorption known and negligible for values of *Chl* greater than 5 $mg{\cdot}m^{-3}$ (note that for such *Chl* values the $b_{bp}(\lambda)$ spectrum can be considered as nearly flat). The phytoplankton absorption coefficient depends on the intracellular pigment composition, but also on the pigment packaging effect of the algal population [*Kirk*, 1975; *Morel and Bricaud*, 1981]. The packaging effect is due to the fact that pigments are not in solution but are packaged within cells, and inside cells, within chloroplasts. This effect, which depends on cell size and intracellular pigment concentration, is function of the wavelength and tends to flatten the phytoplankton absorption spectrum.

[32] The first criterion established to discriminate *P. globosa* from diatoms is based on the position of the maximum of $d\lambda^2 R_{rs}$ within 460–480 nm. The spectral shape of $d\lambda^2 R_{rs}$ presents a maximum centered at 462.5 nm in presence of diatoms, whereas this maximum shifts toward 472.5 nm in presence of *P. globosa*. We suggest that this pattern, also observed on the second derivative of phytoplankton absorption spectra (Figure 3b), can be explained by differences in the intracellular pigment composition. A positive maximum in the $d\lambda^2 R_{rs}$ spectrum, which corresponds to an inflection point in the $R_{rs}(\lambda)$ spectrum, should correspond to a negative minimum in the $d\lambda^2 a_\phi(\lambda)$ spectrum, and then to a maximum in $a_\phi(\lambda)$. The chlorophyll-c_3 (*chl-c*$_3$) is reported as the biomarker of *P. globosa* in the eastern English Channel and southern North Sea, as it appears at generally much higher concentration during *P. globosa* blooms, than during diatom blooms [*Breton et al.*, 2000; *Antajan et al.*, 2004; *Schoemann et al.*, 2005]. While in solvent absorption peaks of chlorophylls-c_{1+2} (*chl-c*$_{1+2}$) and c*hl-c*$_3$ are centered around 446–450 nm and 452 nm [*Jeffrey and Vesk*, 1997], respectively, in vivo absorption maxima of *chl-c*$_{1+2}$ and *chl-c*$_3$ are found around 460 and 467 nm, respectively [*Bidigare et al.*, 1990]. Therefore the shift of the maximum of $d\lambda^2 R_{rs}$ toward longer wavelengths in the presence of *P. globosa* is consistent with a greater proportion of c*hl-c*$_3$ in *P. globosa* than in diatoms.

[33] The second criterion established to discriminate *P. globosa* from diatoms is based on the position of the minimum of $d\lambda^2 R_{rs}$ within 480–510 nm. This minimum characterizes the presence of an inflexion point in the absorption spectrum. We suggest that the position of this inflexion point varies as a function of the relative proportion of *chl-c*$_3$ and carotenoid pigments in the phytoplankton cells. A higher *chl-c*$_3$/*chl-a* ratio and a lower carotenoids/*chl-a* ratio were observed for a *P. globosa* population than for a diatoms population [*Muylaert et al.*, 2006]. While *chl-c*$_3$ absorbs around 467 nm, the carotenoid pigments absorb at a higher wavelength around 500 nm [*Bidigare et al.*, 1990]. Therefore when the proportion of carotenoid pigments decreases (i.e., relatively more *P. globosa*), the position of the inflexion point shifts toward 510 nm. In the same way, when the proportion of *chl-c*$_3$ decreases (i.e., relatively less *P. globosa*), the position of the inflexion point shifts toward 480 nm. This shift may also be intensified during an intensive bloom of *P. globosa*, due to the photoadaptation of the phytoplankton cells, which leads to a decrease of the carotenoids/*chl-a* ratio [*Jonhsen et al.*, 1994; *Stuart et al.*, 2000; *Llewellyn and Gibb*, 2000; *Schluter et al.*, 2000; *Bricaud et al.*, 2004]. The photoadaptation may also partly explain the shift observed between the position of the maximum of the second derivative of $a_{phaeo\text{-}culture}(\lambda)$ (at 493 nm) and the maximum of the second derivative of $a^{ref}_{phaeo\text{-}in\ situ}(\lambda)$ (at 500 nm).

Figure 10. Variation of R_1 as a function of R_2 obtained from numerical simulations performed for the three sensitivity analysis scenarios as described in the text. (a) Scenario I: $a_{CDOM}(443)$ and b_{bp}/b_p are held constant and the *Chl* values vary from 5 to 30 $mg.m^{-3}$. (b) Scenario II: *Chl* and $a_{CDOM}(443)$ are held constant and the b_{bp}/b_p values vary from 0.003 to 0.03. (c) Scenario III: *Chl* and b_{bp}/b_p are held constant and the $a_{CDOM}(443)$ values vary from 10 to 60% of $a(443)$. For each scenario, *w* takes successively the 0, 0.5, and 1 value to simulate an algal population dominated by *P. globosa*, mixed, and dominated by diatoms, respectively.

[34] This study confirms the advantage of a hyperspectral over a multispectral approach to detect different phytoplankton taxonomic groups from remote sensing. The main difference between these two approaches is that, while qualitative information can be provided from the two methods, hyperspectral resolution is needed for quantitative assessment and monitoring of phytoplankton blooms (see Figures 5a, 5b, and 7).

[35] **Acknowledgments.** We are grateful to the crew of the R.V. Côte de la Manche (INSU). We thank Antoine Poteau for his help during measurements. This work was supported by the Centre National D'Etudes Spatiales (CNES), the Conseil Régional du Nord-Pas-de-Calais, and the French National Program of Coastal Environment (PNEC). The different instruments used in this study were funded by the following French programs: ACI and CPER 2001-2006 in the project "Bloom of Phaeocystis" with the support of the Ministry for Research and the Fund European (FEDER). We are also grateful to Emmanuel Boss, Urania Christaki and Cédric Jamet for their valuable comments on the manuscript. We also thank two anonymous reviewers for their pertinent comments on the manuscript.

References

Alvain, S., C. Moulin, Y. Dandonneau, and F. M. Bréon (2005), Remote sensing of phytoplankton groups in case 1 waters from global SeaWiFS imagery, *Deep Sea Res., Part II*, *52*, 1989–2004.

Alvain, S., C. Moulin, Y. Dandonneau, H. Loisel, and F. M. Bréon (2006), A species-dependent bio-optical model of case 1 waters for global ocean color processing, *Deep Sea Res., Part II*, *53*, 917–925.

Antajan, E., M. J. Chretiennot-Dinet, C. Leblanc, M. H. Daro, and C. Lancelot (2004), 19′-Hexanoyloxyfucoxanthin may not be the appropriate pigment to trace occurrence and fate of Phaeocystis: The case of P. globosa in Belgian coastal waters, *J. Sea Res.*, *52*, 165–177.

Astoreca, R. (2007), Study and application of the inherent optical properties of coastal waters from the Phaeocystis-dominated Southern Bight of the North Sea based, Ph.D. thesis, 129 pp., Université Libre de Bruxelles, Brussels, Belgium.

Astoreca, R., V. Rousseau, K. Ruddick, B. Van Mol, J. Y. Parent, and C. Lancelot (2005), Optical properties of algal blooms in an eutrophicated coastal area and its relevance to remote sensing, *Proc. SPIE Int. Soc. Opt. Eng.*, *5885*, 245–255.

Babin, M., D. Stramski, G. M. Ferrari, H. Claustre, A. Bricaud, G. Obolensky, and N. Hoepffner (2003a), Variations in the light absorption coefficients of phytoplankton, non algal particles, and dissolved organic matter in coastal waters around Europe, *J. Geophys. Res.*, *108*(C7), 3211, doi:10.1029/2001JC000882.

Babin, M., A. Morel, V. Fournier-Sicre, F. Fell, and D. Stramski (2003b), Light scattering properties of marine particles in coastal and open ocean waters as related to the particle mass concentration, *Limnol. Oceanogr.*, *48*, 843–859.

Bidigare, R. R., M. E. Ondrusek, J. H. Morrow, and D. A. Kiefer (1990), In vivo absorption properties of algal pigments, *Proc. SPIE Int. Soc. Opt. Eng.*, *1302*, 290–302.

Bouman, H. A., T. Platt, S. Sathyendranath, W. K. W. Li, V. Stuart, C. Fuentes-Yaco, H. Maass, E. P. W. Horne, O. Ulloa, V. Lutz, and M. Kyewalyanga (2003), Temperature as indicator of optical properties and community structure of marine phytoplankton: Implications for remote sensing, *Mar. Ecol. Prog. Ser.*, *258*, 19–30.

Breton, E., C. Brunet, B. Sautour, and J. M. Brylinski (2000), Annual variations of phytoplankton biomass in the eastern English Channel: Comparison by pigment signatures and microscopic counts, *J. Plankton Res.*, *22*, 1423–1440.

Bricaud, A., H. Claustre, J. Ras, and K. Oubelkheir (2004), Natural variability of phytoplankton absorption in oceanic waters: Influence of the size structure of algal populations, *J. Geophys. Res.*, *109*, C11010, doi:10.1029/2004JC002419.

Cadée, G. C. (1992), Phytoplankton variability in the Marsdiep, The Netherlands, *ICES Mar. Sci. Symp.*, *195*, 213–222.

Chen, Z., and P. J. Curran (1992), Derivative reflectance spectroscopy to estimate suspended sediment concentration, *Remote Sens. Environ.*, *39*, 153–166.

Craig, S. E., S. E. Lohrenz, Z. Lee, K. L. Mahoney, G. J. Kirkpatrick, O. M. Schofield, and R. G. Steward (2006), Use of hyperspectral remote sensing reflectance for detection and assessment of the harmful alga, Karenia brevis, *Appl. Opt.*, *45*, 5414–5425.

Cullen, J. J., A. M. Ciotti, R. F. Davis, and M. R. Lewis (1997), Optical detection and assessment of algal blooms, *Limnol. Oceanogr.*, *42*, 1223–1239.

Dick, K., and J. R. Miller (1991), Derivatives analysis applied to high resolution optical spectra of freshwater lakes, paper presented at 14th Canadian Symposium on Remote Sensing, *Can. Remote Sens. Soc.*, Calgary, Alberta, 6–9 May.

Edler, L. (1979), Recommendations for marine biological studies in the Baltic Sea. Phytoplankton and chlorophyll, *Baltic Mar. Biol. Publ.*, *5*, 1–38.

Feldman, G. C., et al. (1989), Ocean color: Availability of global data set, *Eos Trans. AGU*, *70*, 634–641.

Jeffrey, S. W., and M. Vesk (1997), Introduction to marine phytoplankton and their pigment signatures, in *Phytoplankton Pigments in Oceanography*, edited by S. W. Jeffrey, R. F. C. Mantoura, and S. W. Wright, pp. 37–84, UNESCO Pubishing, Paris.

Hamm, C. E. (2000), Architecture, ecology and biogeochemistry of *Phaeocystis* colonies, *J. Sea Res.*, *43*, 307–315.

Jonhsen, G., O. Samset, L. Granskog, and E. Sakshaug (1994), In vivo absorption characteristics in 10 classes of bloom-forming phytoplankton: Taxonomic characteristics and responses to photoadaptation by means of discriminant and HPLC analysis, *Mar. Ecol. Prog. Ser.*, *105*, 149–157.

Kirk, J. T. O. (1975), A theoretical analysis of the contribution of algal cells to the attenuation of light within waters. Part II: Spherical cells, *New Phytol.*, *75*, 21–36.

Kirkpatrick, G. J., O. M. Schofield, D. F. Millie, and M. Moline (2000), Optical discrimination of a phytoplankton species in natural mixed populations, *Limnol. Oceanogr.*, *45*, 467–471.

Leathers, R. A., and T. V. Downes (2004), Self-shading correction for oceanographic upwelling radiometers, *Opt. Express*, *12*, 4709–4718.

Lee, Z., K. L. Carder, and R. A. Arnone (2002), Deriving inherent optical properties from water color: A multiband quasi-analytical algorithm for optically deep waters, *Appl. Opt.*, *41*, 5755–5772.

Le Quéré, C., et al. (2005), Ecosystem dynamics based on plankton functional types for global ocean biogeochemistry models, *Global Change Biol.*, *11*, 2016–2040.

Llewellyn, C. A., and S. W. Gibb (2000), Intra-class variability in the carbon, pigment and biomineral content of prymnesiophytes and diatoms, *Mar. Ecol. Prog. Ser.*, *193*, 33–44.

Loisel, H., J. M. Nicolas, A. Sciandra, D. Stramski, and A. Poteau (2006), Spectral dependency of optical backscattering by marine particles from satellite remote sensing of the global ocean, *J. Geophys. Res.*, *111*(C9), C09024, doi:10.1029/2005JC003367.

Loisel, H., X. Mériaux, J. F. Berthon, and A. Poteau (2007), Investigation of the optical backscattering ratio of marine particles in relation to their biogeochemical composition in the eastern English Channel and southern North Sea, *Limnol. Oceanogr.*, *52*, 739–752.

Louchard, E. M., R. P. Reid, C. F. Stephens, C. O. Davis, R. A. Leathers, T. V. Downes, and R. Maffione (2002), Derivative analysis of absorption features in hyperspectral remote sensing data of carbonate sediments, *Opt. Express*, *10*, 1573–1584.

Lubac, B., and H. Loisel (2007), Variability and classification of remote sensing reflectance spectra in the eastern English Channel and southern North Sea, *Remote Sens. Environ.*, *110*, 45–58, doi:10.1016/j.rse.2007.02.012.

Lubac, B., H. Loisel, A. Poteau, and X. Mériaux (2005), Challenges to identify phytoplankton species in coastal waters by remote sensing, *Proc. SPIE Int. Soc. Opt. Eng.*, *5885*, 235–244.

Menden-Deuer, S., and E. J. Lessard (2000), Carbon to volume relationships for dinoflagellates, diatoms, and other protests plankton, *Limnol. Oceanogr.*, *44*, 154–165.

Millie, D. F., O. M. Schofield, G. J. Kirkpatrick, G. Johnsen, P. A. Tester, and B. T. Vinyard (1997), Detection of harmful algal blooms using photopigments and absorption signatures: A case of the Florida red tide dinoflagellate, Gymnodinium breve, *Limnol. Oceanogr.*, *42*, 1240–1251.

Mobley, C. D., and L. K. Sundman (2001), *Hydrolight 4.2 Technical Documentation*, Sequoia Scientific, WA.

Morel, A. (1974), Optical properties of pure sea water, in *Optical Aspects of Oceanography*, edited by N. G. Jerlov and E. S. Nielsen, pp. 1–24, Academic Press, New York.

Morel, A., and A. Bricaud (1981), Theoretical results concerning light absorption in a discrete medium, and application to specific absorption of phytoplankton, *Deep Sea Res., Part II*, *28*, 1375–1393.

Morel, A., and L. Prieur (1977), Analysis of variations in ocean colour, *Limnol. Oceanogr.*, *22*, 709–722.

Mueller, J. L. (2003), In-water radiometric profile measurements and data analysis protocols, in *Ocean Optic Protocols for Satellite Ocean Color Sensor Validation, Revision 4, Volume III: Radiometric Measurements and Data Analysis Protocols*, NASA Technical Memorandum, edited by J. L. Mueler et al., pp. 7–20, NASA Goddard Space Flight Center, Greenbelt, Md.

Muylaert, K., R. Gonzales, M. Franck, M. Lionard, C. Van der Zee, A. Cattrijsse, K. Sabbe, L. Chou, and W. Vyverman (2006), Spatial

variation in phytoplankton dynamics in the Belgian coastal zone of the North Sea studied by microscopy, HPLC-CHEMTAX and underway fluorescence recordings, *J. Sea Res.*, *55*, 253–265.

Philpot, W. D. (1991), The derivative ratio algorithm: Avoiding atmospheric effects in remote sensing, *IEEE Trans. Geosci. Remote Sens.*, *29*, 350–357.

Platt, T., C. Fuentes-Yaco, and K. Frank (2003), Spring algal bloom and larval fish survival, *Nature*, *423*, 398–399.

Pope, R. M., and E. S. Fry (1997), Absorption spectrum (380–700 nm) of pure water. Part II: Integrating cavity measurements, *Appl. Opt.*, *36*, 8710–8723.

Rousseau, V., D. Vaulot, R. Casotti, V. Cariou, J. Lenz, J. Gunkel, and M. Baumann (1994), The life cycle of *Phaeocystis* (Prymnesiophyseae): Evidence and hypotheses, *J. Mar. Syst.*, *5*, 23–39.

Sathyendranath, S., V. Stuart, G. Cota, H. Maass, and T. Platt (2001), Remote sensing of phytoplankton pigments: A comparison of empirical and theoretical approaches, *Int. J. Remote Sens.*, *22*, 249–273.

Sathyendranath, S., L. Watts, E. Devred, T. Platt, C. Caverhill, and H. Maass (2004), Discrimination of diatoms from other phytoplankton using ocean colour data, *Mar. Ecol. Prog. Ser.*, *272*, 59–68.

Sazhin, A. F., L. F. Artigas, J. C. Nejstgaard, and M. E. Frischer (2007), The colonization of two *Phaeocystis* species (Prymnesiophyceae) by pennate diatoms and other protists: A significant contribution to colony biomass, *Biogeochemistry*, *83*, 137–145, doi:10.1007/s10533-007-9086-2.

Schluter, L., F. Mohlenberg, H. Havskum, and S. Larsen (2000), The use of phytoplankton pigments for identifying and quantifying phytoplankton groups in coastal areas: Testing the influence of light and nutrients on pigment/chlorophyll *a* ratios, *Mar. Ecol. Prog. Ser.*, *192*, 49–63.

Schoemann, V., S. Becquevort, J. Stefels, V. Rousseau, and C. Lancelot (2005), Phaeocystis blooms in the global ocean and their controlling mechanisms, *J. Sea Res.*, *53*, 43–66.

Smith, T. J., G. F. Moore, S. B. Groom, P. E. Land, and T. Tyrrell (2002), Optical modeling and measurements of a coccolithophore bloom, *Appl. Opt.*, *41*, 7679–7688.

Staer, P. A., and J. J. Cullen (2003), Detection of Karenia mikimotoi by spectral absorption signatures, *J. Plankton Res.*, *25*, 1237–1249.

Stuart, V., S. Sathyendranath, E. J. H. Head, T. Platt, B. Irwin, and H. Mass (2000), Bio-optical characteristics of diatom and prymnesiophyte populations in the Labrador Sea, *Mar. Ecol. Prog. Ser.*, *201*, 91–106.

Stumpf, R. P., M. E. Culver, P. A. Tester, M. Tomlinson, G. J. Kirkpatrick, B. A. Pederson, E. Truby, V. Ransibrahmanakul, and M. Soracco (2003), Monitoring Karenia brevis blooms in the Gulf of Mexico using satellite ocean color imagery and other data, *Harmful Algae*, *2*, 147–160.

Subramaniam, A., C. W. Brown, R. R. Hood, E. J. Carpenter, and D. G. Capone (2002), Detecting Trichodesmium blooms in SeaWIFS imagery, *Deep Sea Res., Part II*, *49*, 107–121.

Sun, J., and D. Liu (2003), Geometric models for calculating cell biovolume and surface area for phytoplankton, *Plankton Res. J.*, *25*, 1331–1346.

Tomlison, M. C., R. P. Stumpf, V. Ransibrahmanakul, E. W. Truby, G. J. Kirkpatrick, B. A. Pederson, G. A. Vargo, and C. A. Heil (2004), Evaluation of the use of SeaWIFS imagery for detecting Karenia brevis harmful algal blooms in the eastern Gulf of Mexico, *Remote Sens. Environ.*, *91*, 293–303.

Tsai, F., and W. Philpot (1998), Derivative analysis of hyperspectral data, *Remote Sens. Environ.*, *66*, 41–51.

Van Rijssel, M., C. E. Hamm, and W. W. C. Gieskes (1997), *Phaeocystis globosa* (Prymnesiophyceae) colonies: Hollow structures built with small amounts of polysaccharides, *Eur. Phycol. J.*, *32*, 185–192.

Vantrepotte, V., C. Brunet, X. Mériaux, E. Lécuyer, V. Vellucci, and R. Santer (2007), Bio-optical properties of coastal waters in the Eastern English Channel, *Estuarine Coastal Shelf Sci.*, *72*, 201–212, doi:10.1016/j.ecss.2006.10.016.

Veldhuis, M. J. W., and P. Wassman (2005), Bloom dynamics and biological control of a high biomass HAB species in European coastal waters: A Phaeocystis case study, *Harmful Algae*, *4*, 805–809.

Westberry, T. K., D. A. Siegel, and A. Subramaniam (2005), An improved bio-optical model for the remote sensing of *Trichodesmium* spp. blooms, *J. Geophys. Res.*, *110*, C06012, doi:10.1029/2004JC002517.

R. Astoreca, Université Libre de Bruxelles, Ecologie des Systèmes Aquatiques (ESA), Campus Plaine – CP 221, Boulevard du Triomphe, B-1050 Brussels, Belgium.

L. Felipe Artigas, N. Guiselin, H. Loisel, B. Lubac, and X. Mériaux, Université du Littoral Côte d'Opale, Laboratoire d'Océanologie et de Géosciences (LOG), UMR 8187, MREN - 32 Avenue Foch, 62930 Wimereux, France. (loisel@univ-littoral.fr; bertrandlubac@hotmail.com)